Material flow and thermo-mechanical conditions during Friction Stir Welding of polymers: literature review, experimental results and empirical analysis

F. Simões, D.M. Rodrigues

PII: S0261-3069(13)01171-0
DOI: http://dx.doi.org/10.1016/j.matdes.2013.12.038
Reference: JMAD 6126

To appear in: *Materials and Design*

Received Date: 27 October 2013
Accepted Date: 16 December 2013

Please cite this article as: Simões, F., Rodrigues, D.M., Material flow and thermo-mechanical conditions during Friction Stir Welding of polymers: literature review, experimental results and empirical analysis, *Materials and Design* (2013), doi: http://dx.doi.org/10.1016/j.matdes.2013.12.038

Material flow and thermo-mechanical conditions during Friction Stir Welding of polymers: literature review, experimental results and empirical analysis

F. Simões[1,2], D. M. Rodrigues[2,*]

[1]Instituto Politécnico de Coimbra, ISEC, DEM, Portugal.

[2]CEMUC – Department of Mechanical Engineering, University of Coimbra, Portugal.

*e-mail: dulce.rodrigues@dem.uc.pt, tel. + (351) 239 790 700, fax. + (351) 239 790 701

Abstract

Meanwhile the thermo-mechanical conditions during Friction Stir Welding (FSW) of metals have already been subject of extensive analysis and thoroughly discussed in literature, in which concerns the FSW of polymers, the information regarding this subject is still very scarce. In this work, an analysis of the material flow and thermo-mechanical phenomena taking place during FSW of polymers is performed. The analysis is based on a literature review and on the examination of friction stir welds, produced under varied FSW conditions, on polymethyl methacrylate (PMMA). Due to the high transparency of this polymer, it was possible to analyse easily the morphological changes induced by the welding process on it. Results of the weld morphologic analysis, of the residual stress fields in the different weld zones and of temperature measurements during welding are shown, and its relation with welding conditions is discussed. From the study it was possible to conclude that, due to the polymers rheological and physical properties, the thermo-mechanical conditions during FSW are very different from that registered during welding of metals, leading to completely different material flow mechanisms and weld defect morphologies.

Keywords: Friction Stir Welding; Polymers; PMMA; Morphology; Residual stresses; Temperature

Introduction

Although friction stir welding (FSW) process was initially developed for the joining of Al-alloys [1], a large number of studies addressing similar and dissimilar FSW of other metallic materials were also already developed [2, 3]. However, in which concerns the joining of polymers by FSW, the amount of work performed is still very small and most of the studies published were developed considering a very narrow range of polymers, more precisely, polyethylene (PE) [4–10], high density polyethylene (HDPE) [4, 11, 12], polypropylene (PP) [13 -15], acrylonitrile-butadiene-styrene (ABS) [16], polyethylene-terephthalate-glycol (PETG) [17] and the polyamide Nylon 6 [18]. Those works can be divided in two categories, according to the type of FSW tool in use, i.e., works in which are used conventional FSW tools [4-7; 10-12; 15; 18], similar to that used in FSW of metals, and works in which stationary shoulder tools are used [8, 9, 13, 16, 17].

In literature it is also possible to find a relatively large number of works addressing the joining of polymers using Friction Stir Spot Welding (FSSW), which is a FSW related technique. The FSSW process involves only the plunge and retraction of the FSW tool, being exclusively used in discontinuous lap joining. The works already performed on FSSW addressed the joining of high density polyethylene (HDPE) [19-21], polypropylene (PP) [22-24] and polymethyl methacrylate (PMMA) [25]. The dissimilar joining of PMMA to Acrylonitrile-butadiene-styrene (ABS) was also investigated [26].However, despite the growing interest of the FSSW technique, the following review will exclusively address the works performed using the FSW technology, which is the one explored in the experimental program conducted in present work.

Bozkut [4] employed a conventional FSW tool, with a 18 mm diameter shoulder and a 6 mm diameter pin, in the welding of high density polyethylene (HDPE). The tool rotation speed (ω) and the traverse speed (v) ranged between 1500-3000 rpm and 45-115 mm/min, respectively. This author measured temperature variations between 120 and 165 ºC during FSW of this polymer which has a melting temperature of 132ºC. The author observed voids and root cracks in the welds, which were responsible for their poor tensile properties.

An investigation on the effects of critical process parameters on FSW of polyethylene was also performed by *Saeedy and Givi* [10], who tested rotational speeds and welding speeds ranging from 1000 to 1800 rpm and 12 to 20 mm/min, respectively, and tool tilt angles of 1° and 2°. An optimum weld strength value of 75% of that of the base material was achieved in this study, but for only one optimized set of welding parameters. These results showed the important influence of process parameters on welding results. The same was concluded by *Rezgui et al.* [12] who used ANOVA in optimizing FSW process parameters for the joining of HDPE.

Arici and Selale [5] and *Arici and Sinmaz* [6] also performed FSW of PE using conventional FSW tools. In order to avoid root crack defects, such as that reported by *Bozkurt* [4], these authors performed double pass butt welding and used rotation speeds up to 1000 rpm and traverse speeds up to 60 mm/min. They reported insufficient heat generation for rotation speeds of 600 and 800 rpm and suitable welding conditions at 1000 rpm. Those authors also observed that, depending on the amount of heat input, some material was expelled from the joining area during welding. In which concerns the double pass FSW, *Arici and Selale* [5] also studied the effect of tool tilt angle on FSW of PE observing that the thickness of the welds, as well as the tensile strength, decreased with increasing tool tilt angle.

Aydin [7] used a tool and process parameters similar to that used by *Arici and Selale* [5], but performed single pass butt welding with pre-heating of the base material. They report that pre-heating insures adequate heating even at low rotation speeds. Welds surface morphology and global properties were also appointed to be improved by pre-heating. The use of pre-heating in FSW of polyethylene, with conventional rotating tools, was also studied by *Squeo and Quadrini [11]*, who performed pre-heating of the tool, as well as pre-heating of the plates to be joined. Two different pin diameters were tested and several combinations of tool traverse and rotational speeds. As the previous authors, *Squeo and Quadrini* also conclude that pre-heating of the tool enabled improving welds quality. However, according to the authors, achieving optimum FSW conditions still needed further optimization of process parameters.

Panneerselvam and Lenin [15] used conventional FSW tools to analyse the influence of pin geometry on FSW results, but using PP as base material. They tested square, triangular, threaded and tapered pin geometries, in a range of rotation speeds varying from 1500 to 2250 rpm and traverse speeds varying from 30 to 60 mm/min. According to the pin geometry and welding parameters, several defects were reported, such as lack of consolidation, porosities, cavities and inclusions. Poor joining was also reported to occur mainly at the retreating side of the welds. The authors claim that the threaded tool pin profile generated the best welding results.

Finally, Panneerselvam and Lenin [18] conducted FSW tests, using a conventional rotating tool, as in previous works, but testing a different base material, the Nylon 6 polyamide. These authors used a specially designed left hand threaded tool pin profile, operated at a rotational speed of 1000 rpm and at a welding speed of 10 mm/min, to analyse the influence of tool rotation direction on weld quality. They found that the FSW joints fabricated with the tool operating with counter clockwise rotation were free of defects and had improved strength, relative to the welds performed with clockwise tool rotation. They attributed the poor quality of the welds obtained with the clockwise rotating tool to the expulsion of the stirred material from the weld seam.

In order to avoid some of the problems registered in FSW with conventional tools, such as the squeezing of the melted polymer from the weld nugget, some researchers developed modified tools, with a stationary shoulder, sometimes called “shoe”. *Mostafapour and Azarsa* [8], for example, used a stationary aluminium shoulder, heated by electric resistance, to weld high-density polyethylene (HDPE). Shoulder temperatures were adjusted to 80, 110 and 140ºC. The pin was threaded, with 10 mm diameter. The rotation speeds tested ranged between 1000 to 1600 rpm and the traverse speeds between 10 to 40 mm/min. According to the authors, due to the low thermal conductivity of the polymer, the heat generated during welding was concentrated in the weld nugget, resulting in the formation of a pool of semi-molten polymer around the pin. The size of the molten pool was increased by increasing the rotation speed, resulting in improved tool stirring action and weld quality. However, when the shoulder temperature was set to 80ºC and 110ºC, weld

material degradation was observed. Incomplete tool penetration and lack of connection between the weld nugget and the adjacent base material were the main defects reported. Defect incidence was observed to be reduced when the heat input was sufficient to melt the whole nugget material.

Rezgui et al [9] also used a stationary shoulder tool to weld HDPE, but with a shoulder made of wood, and three cylindrical threaded pins (M10, M12 and M14). The Taguchi method was used by the authors to optimize the FSW parameters. Rotation speeds from 900 to 1700 rpm and traverse speeds from 16 to 44 mm/min were selected. They reported that welding took place by melting the polymer and that the low thermal conductivity of this material was responsible for the formation of a small size HAZ. The tensile behaviour of the welds was analysed, being referred that the presence of discontinuities in the weld caused specimens failure for very small strain values.

Kiss and *Czigány* [13, 17] performed FSW using a non-heated PTFE stationary shoulder and different pin diameters and FSW parameters. In order to analyse the internal stresses, using stress optics, as well as to visualize the weld nugget and HAZ, those authors changed the base material from PP (semicrystalline), to PETG, which displays a high level of transparency and low crystallization tendency. For the PP welds, no significant differences were reported by the authors between the advancing and retreating sides of the welds. Spherulitic structures, similar to that of the base material, were observed in the nugget, which they attributed to the slow cooling rate of the weld. Concerning to the PETG welds, it was reported the presence of a sharp discontinuity between the weld and the base material. The colour fringes, registered in the stress optics photographs, were attributed by the authors to the molecular orientation induced by tool rotation and to the residual stresses resulting from heating.

Finally, *Bagheri et al*. [16], used a stationary shoulder tool with an heated shoe (T=50; 80; 100ºC) and a non-conventional threaded pin, 10 mm in diameter and 7 mm in pitch, to weld ABS. The rotational speeds used were 800, 1250 and 1600 rpm and the traverse speeds were 20, 40 and 80 mm/min. It was concluded that increasing the rotational speed, conducted to an important increase in temperature that lead to burning of the work piece and squeezing of melted material

from the weld. On the other hand, for low rotation speeds, inadequate material mixing and lack of joining between the weld and the base material were observed. In the same way, at the highest travel speeds, the weld line was observed to be very discontinuous. Those results were improved by heating the shoe. The maximum tensile strength welds were produced with the shoe heated to 100ºC. However, despite the optimized welding conditions, the tensile samples were observed to fail at the retreating side of the welds, were a discontinuity was present. The maximum tensile strength was reported for the welds performed with the maximum heat input, i.e., maximum tool rotation speed and shoe temperature and the lowest traverse speed.

From the literature review on FSW it becomes apparent that in order to obtain good quality welds, stationary shoulder tools should be used [8, 9, 13, 16, 17]. Using this type of tools, the rotating pin generates the friction heat necessary to melt and weld the abutting surfaces by solidification. The stationary shoulder also avoids the plastic material, swirling around the pin, of being expelled from the weld seam [13]. High shoulder temperature and high tool rotational speeds, conducting to base materials melting and slow cooling of the welds, are indicated as important factors in achieving successful welding [8, 16]. However, since melting is involved in materials joining, the FSW of polymers, unlike the FSW of metals, can't be considered a solid state welding process. Another important issue is that in spite of the well-established, and patented, tools and procedures for the FSW of polymers, no systematic knowledge on material flow mechanisms and thermo-mechanical conditions during FSW, which implies analysing the temperature distribution and stress-strain evolution during welding, as well as its relation with processing parameters and defect formation, can be found in literature. In current work, the material flow and thermo-mechanical conditions during FSW of polymers are analysed by comparison with the metalworking flow-partitioned model proposed by Arbegast [27].

Despite the absence of publications on material flow during FSW of polymers, several works can be found in literature analysing material flow during similar [28-37] and dissimilar [38-44] FSW of metals. Those works describe the different methodologies used to analyse the flow

mechanisms (experimental and numerical simulation procedures) and address a varied range of welding conditions, i.e., different base materials, tool geometries and process parameters. The Arbegast flow partitioned model [27], cleverly synthetizes the main flow mechanisms identified in that literature, and for that reason, was selected in current work for performing a comparative analysis on material flow in FSW of polymers and metals.

Experimental Procedure

Bead on plate friction stir welds on 10 mm thick PMMA plates were made in a CNC machine. In Table 1 are shown the thermal properties of the base material [45] which are considered relevant in present analysis. It is interesting to stress that the heating and cooling of the metallic and polymeric materials are substantially different, due to the large difference in thermal conductivity. For instance, the PMMA thermal conductivity presented in Table 1 (0,17 to 0,25 W/m.ºC) is only 0.13% of aluminium alloys thermal conductivity (around 135 W/m.ºC).

By performing bead on plate welding it was possible to simplify the experimental work, excluding simultaneously the influence of plates clamping and positioning on welding results. As shown in Figure 1, two different left-hand thread tools were used. Tool 1 is a conventional FSW tool, with a 15 mm conical shoulder and a 5 mm cylindrical pin. Tool 2 is a 35 mm diameter shoulder tool, with a flat base on the outside and a conical geometry in the center, and a 6 mm cylindrical pin. The inner conical cavity in tool 2 shoulder was used in order to avoid the material of being expelled from the joint during welding. The pin length, of 6 mm, was the same for both tools. By using a pin length lower than the PMMA plates thickness it was possible to have a full picture of the heat and material transfer under the pin during welding.

The same advancing speed, of 25 mm/min, and rotation speed, of 700 rpm, were used for both tools. During welding, the temperature evolution at the surface of the weld beads was registered using a infrared camera from Flir, model ThermaCAM E300, that produces fully radiometric images, allowing to measure the temperature of objects. Transverse and longitudinal

samples were cut, as schematized in Fig. 2, from several welds in order to enable a deep analysis of the welds morphology. Due to the high transparency of the PMMA, a qualitative photoelastic analysis of the residual stress fields in the welds was accomplished by using a polarized light device.

Weld morphology analysis

In order to characterize the main features of the polymeric welds, in Fig.3 is show an image of the surface of a weld, produced with tool 1. In this figure it is possible to clearly distinguish the pin influence zone, in the centre, surrounded by a well-defined shoulder influence zone. Meanwhile the pin influence zone displays the characteristic FSW arc shaped striations, resulting from the periodic deposition of material, by the pin, at the trailing side of the tool, the shoulder influence zone displays a very smooth surface with no evidence of material stirring, into the pin influence zone, during welding. Tool 2 surface displayed similar surface morphology.

In Figs. 4 and 5 are shown two (Fig. 4.a and 5.a) and three (Fig. 4.b and 5.b) dimensional images of tool 1 and tool 2 transverse weld samples, respectively. In both figures are discernible important differences in morphology between the advancing and retreating sides of both welds. Meanwhile the advancing side material displays the same full transparency features of the original base material, with only very small and dispersed discontinuities, indicating an almost perfect merging between the weld and the adjacent materials, the retreating side material is fully non-transparent, displaying a straight interface between the pin influence zone and the adjacent material. In Fig.6, where are shown images of tool 1 longitudinal samples, which illustrate individually the retreating (Fig. 6.a) and advancing (Fig. 6.b) sides of the weld, it is possible to confirm that those characteristics are repeated consistently along the weld. Optical microscopy images of the non-transparent retreating side material in Fig. 6.a, are shown in Fig 7 showing that this feature results from the presence of a large number of macro and micro voids in its structure.

In Figs.8.a and 8.b are now shown backlight images of the same welds, which enable to distinguish not only the same features already addressed when analysing Figs.4 to 6, i.e., a straight interface between the pin influence zone at the retreating side of the weld, with a portion of opaque material next to it, but also a less pronounced interface at the advancing side of the weld, which was not perceptible in the previous figures. No signs of material being stirred by the shoulder, across that interface, into pin influence zone, are perceptible in both figures, as usually reported for the friction stir welds in metals. So, the straight interface at the retreating side of both welds indicates that the thermo-mechanical affected zone (TMAZ), for the polymeric materials, is restricted to the pin influence zone. The backlight images also display, for both welds, the presence of a heat affected zone (HAZ) surrounding the TMAZ. For both welds, the HAZs displays a perfectly regular and well defined geometry, extending from the under shoulder area to the bottom of the pin. Unlike the TMAZ, the HAZ displays perfectly symmetrical features for both welds, reflecting the symmetry in heat production and dissipation under the shoulder. Finally, in Figs 8.c and 8.d are shown polarized light images of the welds in Figs. 8.a and 8.b, revealing the residual stress fields induced by the welding process. Like the TMAZ morphology, the residual stress field in its neighbourhood, is also not symmetric for both welds, being possible to notice a stress concentration at the advancing side of the TMAZ for both welds. In spite of this, for the tool 2 weld, the residual stress fields discernible in the HAZ located at the outer side of the shoulder influence zone have symmetrical features.

Analysis of the thermo-mechanical conditions during FSW of polymers

According to Arbegast studies on FSW of metals [27], and as is schematized in Fig. 9.a, material processing during welding progresses sequentially from a pre-heating phase, at the leading side of the tool, followed by the initial deformation, extrusion and forging of the stirred material under the tool, and finally, by its cool-down at the trailing side of the tool. Due to the very low thermal conductivity of the polymers, the pre-heating and initial deformation areas in front of the tool are

shrunk in a thin layer, as is shown in Fig. 9.b, and the final cool down of the weld is very slow as shown in Fig 10.a and 10.b, where the temperature fields registered at the surface of the plate, with a infrared camera, during FSW, is represented. According to Fig. 10.b, where are shown temperatures profiles at the trailing side of the tool, the temperature there remain high even after a significant tool displacement.

Arbegast [27] also stated that, for metals, the material flow at the trailing side of the tool is partitioned in four distinct deformation zones, distributed around the pin and beneath the shoulder, as it is shown in Fig. 11.a. The advancing (Zone I) and retreating (Zone II) material deformation zones form inside the pin influence zone. Due to tool rotation, Zone II material converges to Zone I, by flowing around the pin and downward it, through Zone IV. Zone III material, in the shoulder influence zone, is also dragged across the top toward the advancing side Zone 1.The size and shape of each material flow zone represented in Fig. 11.a is related to the temperature field, the constitutive properties of the materials being joined, the strain rate and the tool geometry. Arbegast related inadequacies in this flow partitioning to specific FSW features and defect types.

Coupling the weld morphological analysis performed in the previous item, for the PMMA welds, with the Arbegast flow-partitioned deformation zone model for welds in metals, it becomes possible to access the thermo-mechanical conditions during FSW of polymers, as well as to understand the mechanisms of defect formation for these materials. Actually, comparing the cross section of the polymer weld in Fig. 11.b, with Arbegast model in Fig. 11.a, it becomes apparent that Zone III is absent from the polymeric welds. Effectively, the interface of the pin influence zone remains straight, and parallel to the pin profile, from the bottom to the top of the welds, which means that no material flow could have took place across it. This assumption is also in accordance with figure 3 where it is possible to distinguish, clearly delimited, the shoulder and pin influence zones at the top of the weld. In the same way, the straight line at the bottom of the TMAZ, discernible in Figs. 8.a and 8.b, indicates that Zone IV is also absent from the friction stir welds in PMMA.

Analysing again the temperature distribution at the trailing side of the tool, represented in Fig. 10, and taking into account the table 1, it is possible to conclude that, during FSW, the temperatures under the shoulder were higher than 135ºC, which means that polymer melting should have took place in contact with the shoulder. Most of this melted material is squeezed from the under shoulder area under the centrifugal action of the rotating tool, instead of entering into Zone I, which explains the absence of Zone III from the PMMA weld profiles. Actually, it is possible to see some lack of material at the top of all welds. As observed in current work, *Panneerselvam and Lenin* [18], *Arici and Selale* [5] and *Bagheri et al.* [16] also reported material ejection from the weld seam during FSW. According to *Panneerselvam and Lenin* [18], in FSW with conventional shoulder tools, this phenomenon may be avoided by welding with a left hand threaded pin operating in counter clockwise direction. In FSW with stationary shoulder tools, according to *Bagheri et al.* [16], the burning and ejection of the polymer from the weld bead can be avoided by an appropriate control of the rotation speed.

Analysing again Fig.11.b it is possible to see that the non-transparent material at the retreating side of the welds (Zone II) displays features which indicate that the material flows from it to the advancing side of the tool (Zone I), which is in accordance with Arbegast model. The magnification view of the non-transparent material of Zone II, shown in Fig. 7, also shows that this material has a deeply non-homogeneous structure, with large voids inside of it. Assuming that material melting occurs not only in the under shoulder area, but also in the pin influence zone, it is reasonable to accept that melted material is also squeezed out of the weld from this zone. This will occur more easily at the retreating side of the tool, were the tangential flow of the material is opposite to the traverse speed of the tool. The squeeze of melted material to the under shoulder zone III, by one side, and to the advancing side Zone I, by the other side, originate the severe discontinuities reported in Figs. 7. At the advancing side of the tool, where the partially melted material coming from the retreating side is extruded against the base material side wall, the pressure generated by the flow of material is sufficient to consolidate it, giving rise to the almost continuous

joint interface shown in figures 4 to 6. It is important to stress that in FSW of metals, the advancing side of the weld is the preferential location for defect formation [46-50], which is opposite to that registered in current work for the polymer welds. The formation of important discontinuities at the retreating side of the polymer friction stir welds can also be observed in most of the works published by other authors, but is only explicitly mentioned in references [15, 16]. An important question is whether the retreating side discontinuities can be avoided by performing the welds at lower temperatures, avoiding in that way material squeezing due to melting. In figure 12.a is shown an image of a cross-section of the initial part of a tool 2 weld. Since no dwell time was used, this part of the weld, performed with the tool still cold, can be considered a "low" temperature weld. As it is possible to see from the picture, no important discontinuities can be reported at both the advancing and retreating sides of this part of the weld, which supports the hypothesis that the defects results from melting and squeezing of material from the weld bead. However, in Fig. 12.b is shown another image of the same sample, but acquired one month after cutting the sample. In this image is now possible to see, two thin cracks, located at the advancing and retreating sides of the weld. Those cracks, which result from the residual stress field in the weld, revealed by the polarized light image of Fig. 8.d, show that residual stresses can be very important in FSW of polymers.

Conclusions

From current analysis important differences in material flow and temperature distribution between metallic and polymeric materials, during FSW, were identified and critically analysed based on Arbegast flow-partitioned deformation zone model. The differences in thermo-mechanical conditions are explained based on the strong dissimilarities in weld morphology and defect location. Meanwhile for metals the welds result from the confluence of the pin and shoulder driven flow volumes in the TMAZ, for polymers, only the pin driven flow volume enters the TMAZ, since the shoulder driven material, melted during welding, is squeezed from the joint. The formation of

important discontinuities, at the retreating side of the welds, indicated in literature as one of the main weldability problems for polymers, is also explained by the squeezing of melted material from both the shoulder and pin driven flow volumes.

Acknowledgements: This research is sponsored by FEDER funds through the program COMPETE – Programa Operacional Factores de Competitividade – and by national funds through FCT – Fundação para a Ciência e a Tecnologia –, under the project PEst-C/EME/UI0285/2013.

References

[1] Threadgill PL, Leonard AJ, Shercliff HR, Withers PJ. Friction stir welding of aluminium alloys. International Materials Reviews 2009; 52(2): 49 – 93.

[2] DebRoy T, Bhadeshia HKDH. Science and Technology of Welding and Joining 2010; 15(4): 266 – 270.

[3] Çam G. Friction stir welded structural materials: beyond Al-alloys. International Materials Reviews 2011; 56: 1 – 48.

[4] Bozkurt Y. The optimization of friction stir welding process parameters to achieve maximum tensile strength in polyethylene sheets. Materials and Design 2012; 35: 440 – 445.

[5] Arici A, Selale S. Effects of tool tilt angle on tensile strength and fracture locations of friction stir welding of polyethylene. Science and Technology of Welding and Joining 2007; 12: 536 – 539.

[6] Arici A, Sinmaz T. Effects of double passes of the tool on friction stir welding of polyethylene. Journal of Materials Science 2005; 40: 3313–3316.

[7] Aydin M. Effects of Welding Parameters and Pre-Heating on the Friction Stir Welding of UHMW-Polyethylene. Polymer-Plastics Technology and Engineering 2010; 49: 595–601.

[8] Mostafapour A, EAzarsa E. A study on the role of processing parameters in joining polyethylene sheets via heat assisted friction stir welding: Investigating microstructure, tensile and flexural properties. International Journal of the Physical Sciences 2012; 7(4): 647 – 654.

[9] Rezgui A, Ayadi M, Cherouat A, Hamrouni K, Zghal A, Bejaoui S. Application of Taguchi approach to optimize friction stir welding parameters of polyethylene. EPJ Web Conference 2010; 6: 1 – 8.

[10] Saeedy S, Givi M. Investigation of the effects of critical process parameters of friction stir welding of polyethylene. Proceedings of the Institution of Mechanical Engineers, Part B: Journal of Engineering Manufacture 2011; 225 (8): 1305-1310.

[11] Squeo E, Quadrini F. Friction Stir Welding of Polyethylene Sheets. The Annals of "DUNĂREA DE JOS" University of Galati Fascicle V, Technologies in Machine Building 2009; ISSN 1221- 4566.

[12] Rezgui M, Trabelsi A, Ayadi A, Hamrouni K. Optimization of Friction Stir Welding Process of High Density Polyethylene. International Journal of Production and Quality Engineering 2011; 2 (1): 55-61.

[13] Kiss Z, Czigány T. Microscopic analysis of the morphology of seams in friction stir welded polypropylene. Express Polymer Letters 2012; 6: 54 – 62.

[14] Kiss Z, Czigány T. Applicability of friction stir welding in polymeric materials. Periodica polytechnica Mechanical Engineering 2007; 51: 15 – 18.

[15] Panneerselvam K, Lenin K. Effects and defects of the polypropylene plate for different parameters in friction stir welding process. International Journal of Research in Engineering and Technology 2013; 2(2): 143 – 152.

[16] Bagheri A, Azdast T, Doniavi A. An experimental study on mechanical properties of friction stir welded ABS sheets. Materials and Design 2013; 43: 402 – 409.

[17] Kiss Z, Czigány T. Effect of Welding Parameters on the Heat Affected Zone and the Mechanical Properties of Friction Stir Welded Poly(ethylene-terephthalate-glycol). Journal of Applied Polymer Science 2012; 125: 2231–2238.

[18] Panneerselvam K, Lenin K. Joining of Nylon 6 plate by friction stir welding process using threaded pin profile. Materials and Design 2014; 53: 302-307.

[19] Bilici M, Yükler A. Influence of tool geometry and process parameters on macrostructure and static strength in friction stir spot welded polyethylene sheets. Materials and Design 2012;33:145–152.

[20] Bilici M, Yükler A, Kurtulmus M. The optimization of welding parameters for friction stir spot weldingof high density polyethylene sheets. Materials and Design 2011; 32: 4074–4079.

[21] Bilici M, Yükler A. Effects of welding parameters on friction stir spot welding of high density polyethylene sheets. Materials and Design 2012; 33:545–550.

[22] Bilici M. Effect of tool geometry on friction stir spot welding of polypropylene sheets. Express Polymer Letters 2012; 6 (10): 805–813.

[23] Mert S, Arici A. Design of optimal joining for friction stir spot welding of polypropylene sheets. Science and Technology of Welding and Joining 2011; 16 (6):522–527.

[24] Arici A. Friction stir spot welding of polypropylene. Journal of Reinforced Plastics and Composites 2008; 27 (18): 2001–2004.

[25] Oliveira P, Amancio-Filho S, Santos J, Hage E. Preliminary study on the feasibility of friction spot welding in PMMA. Materials Letters 2010; 64: 2098–2101.

[26] Dashatan S, Azdast T, Ahmadi S, Bagheri A. Friction stir spot welding of dissimilar polymethyl methacrylateand acrylonitrile butadiene styrene sheets. Materials and Design 2013; 45: 135–141.

[27] William J. Arbegast. A flow-partitioned deformation zone model for defect formation during friction stir welding. Scripta Materialia 2008; 58: 372–376.

[28] Colligan K. Material Flow Behavior during Friction Stir Welding of Aluminum. Welding Journal 1999; 78 (7): 229s–237s.

[29] Seidel T, Reynolds A. Visualization of the material flow in AA2195 friction-stir welds using a marker insert technique. Metallurgical and Materials Transactions A 2001; 32A: 2879-2884.

[30] Guerra M, Schmidt C, McClure JC, Murr L, Nunes A. Flow patterns during friction stir welding. Materials Characterization 2003; 49: 95 -101.

[31] Fratini L, Buffa G, Palmeri D, Hua J, Shivpuri R. Material flow in FSW of AA7075-T6 butt joints: numerical simulations and experimental verifications. Science and Technology of Welding and Joining 2006; 11: 412-421.

[32] Schmidt H, Dickerson T, Hattel J. Material flow in butt friction stir welds in AA2024-T3. Acta Materialia 2006; 54: 1199- 1209.

[33] Zhao Y, Lin S, Qu F, Wu L. Influence of pin geometry on material flow in friction stir welding process. Materials Science and Technology 2006; 22: 45-50.

[34] Leitão C, Leal R., Rodrigues D, Vilaça P, Loureiro A. Material flow in friction stir welding, Microscopy and Microanalysis 2008, 14: 87-90.

[35] Chen Z, Pasang T, Qi Y. Shear flow and formation of Nugget zone during friction stir welding of aluminium alloy 5083-O. Materials Science and Engineering A 2008 ; 474: 312-316.

[36] Lorrain, O, Favier, V, Zahrouni, H, Lawrjaniec, D. Understanding the material flow path of friction stir welding process using unthreaded tools, Journal of Materials Processing Technology 2010; 210 (4): 603-609.

[37] Fonda R, Reynolds A, Feng C, Knipling, K, Rowenhorst D. Material flow in friction stir welds. Metallurgical and Materials Transactions A 2013; 44 (1):337-344.

[38] Li Y, Murr L, McClure J. Solid-state flow visualization in the friction-stir welding of 2024 Al to 6061 Al. Scripta Materialia 1999; 40:1041-1046.

[39] Li Y, Murr L, McClure J. Flow visualization and residual microstructures associated with the friction-stir welding of 2024 aluminum to 6061 aluminum. Materials Science and Engineering A 1999; 271:213-223.

[40] Guerra M, Schmidt C, McClure J, Murr L, Nunes A. Flow patterns during friction stir welding. Materials Characterization 2003; 49: 95-101.

[41] Leal R, Leitão C, Loureiro A, Rodrigues D, Vilaça P. Material Flow in heterogeneous friction stir welding of thin aluminium sheets: Effect of shoulder geometry. Materials Science and Engineering A 2008; 498 (1-2): 384–391.

[42] Galvão I, Leal R, Loureiro A, Rodrigues D. Material flow in heterogeneous friction stir welding of aluminium and copper thin sheets. Science and Technology of Welding and Joining 2010; 15 (8): 654-660.

[43] Esmaeili A, Besharati Givi, M, Zareie Rajani H. Experimental investigation of material flow and welding defects in friction stir welding of aluminum to brass. Materials and Manufacturing Processes 2012; 27 (12): 1402-1408.

[44] Pourahmad P, Abbasi M. Materials flow and phase transformation in friction stir welding of Al 6013/Mg. Transactions of Nonferrous Metals Society of China 2013; 23 (5): 1253-1261.

[45] Ashby M. CES Edupack 2009, Granta Design.

[46] C. Leitão, R. Louro, D.M. Rodrigues. Analysis of high temperature plastic behaviour and its relation with weldability in friction stir welding for aluminium alloys AA5083-H111 and AA6082-T6. Materials and Design 2012; 37, 402-409.

[47] Kim Y, Fujii H, Tsumura T, Komazaki T, Nakata K. Three defect types in friction stir welding of aluminum die casting alloy. Materials Science and Engineering A 2006; 415: 250-254.

[48] Chen H, Yan K, Lin T, Chen S, Jiang C, Zhao Y. The investigation of typical welding defects for 5456 aluminum alloy friction stir welds. Materials Science and Engineering A 2006; 433: 64-69.

[49] Iordachescu M, Iordachescu D, Ocana J, Vilaça P, Scitelnicu E. Characteristic flaws in aluminium alloys joints. Metalurgia International 2009; 12, 135-138.

[50] Kumar K, Kailas S. The role of friction stir welding tool on material flow and weld formation. Materials Science and Engineering A 2008; 485: 367-374.

Table Captions

Table 1 –Thermal properties of PMMA cast sheet [15].

Glass temperature (°C)	Maximum service temperature (°C)	Minimum service temperature (°C)	Thermal conductivity (W/m °C)
96-104	80-105	-75 to -65	0.17-0.25

Figure Captions

Figure 1 – Schematic representation of FSW tool geometries.

Figure 2 – Weld sampling scheme.

Figure 3 – Picture of the surface of a weld produced with tool 1.

Figure 4 – Two (a) and three (b) dimensional images of tool 1 weld.

Figure 5 – Two (a) and three (b) dimensional images of tool 2 weld.

Figure 6 – Longitudinal tool 1samplesdisplaying the retreating (a) and the advancing (b) side.

Figure 7 – Optical microscopy image of the retreating side material, showing macro and micro voids developed during FSW.

Figure 8 - Backlight and polarized light images of tool 1 (a and c) and tool 2 (b and c) welds.

Figure 9-Schematic representation of Arbegast model [14] for FSW of metals (a) and longitudinal sections of tool 1 sample (b).

Figure 10 -Tool and material image captured with a infrared camera after FWS (a) and temperature fields surface and temperature profile at different weld positions (b).

Figure 11 -Representation of deformation zones and flow material for FSW of metals according Arbegast model (a) and transverse sections of Tool 1 sample (b).

Figure 12 -Optical microscopy image of the sample after welding (a) and image of the weld one month after welding (b) showing additional defects.

Figure 1 – Schematic representation of FSW tool geometries

Figure 2 – Weld sampling scheme

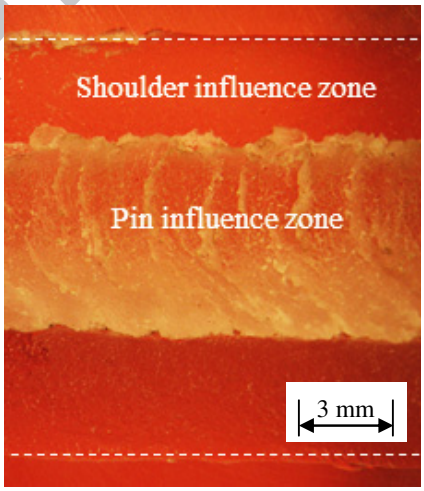

Figure 3 – Picture of the surface of a weld produced with tool 1.

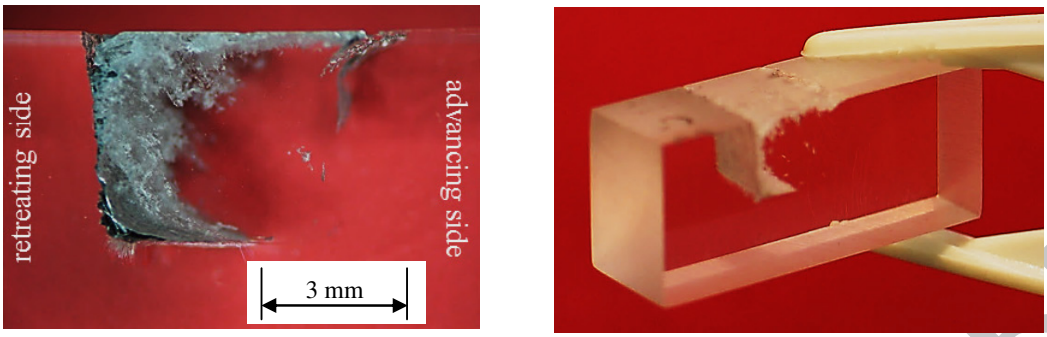

(a) (b)

Figure 4 – Two (a) and three (b) dimensional images of tool 1 weld

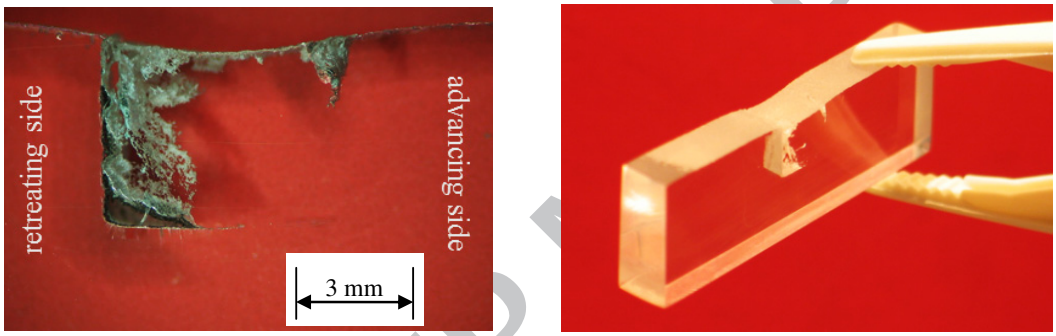

(a) (b)

Figure 5 – Two (a) and three (b) dimensional images of tool 2 weld

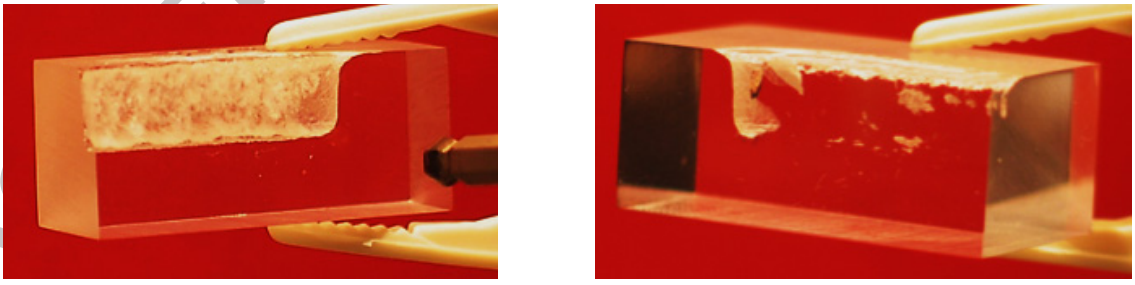

(a) (b)

Figure 6 – Longitudinal tool 1 samples displaying the retreating (a) and the advancing (b) side

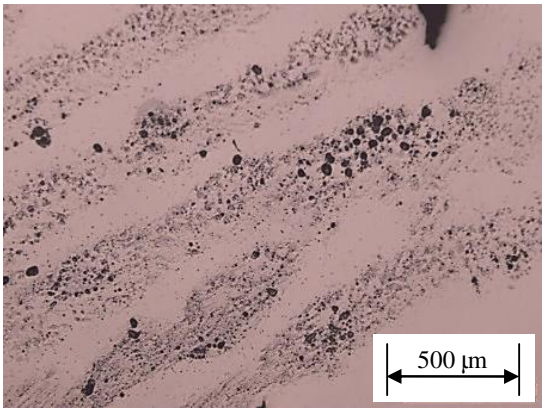

Figure 7 – Optical microscopy image of the retreating side material, showing macro and micro voids developed during FSW.

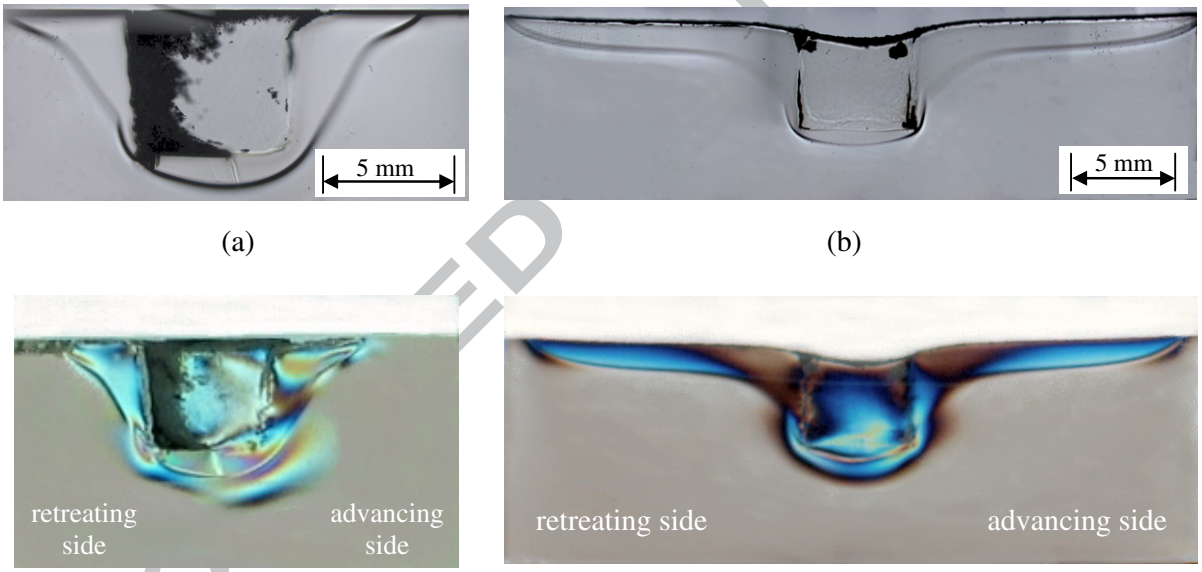

(a) (b)

(c) (d)

Figure 8 - Backlight and polarized light images of tool 1 (a and c) and tool 2 (b and c) welds.

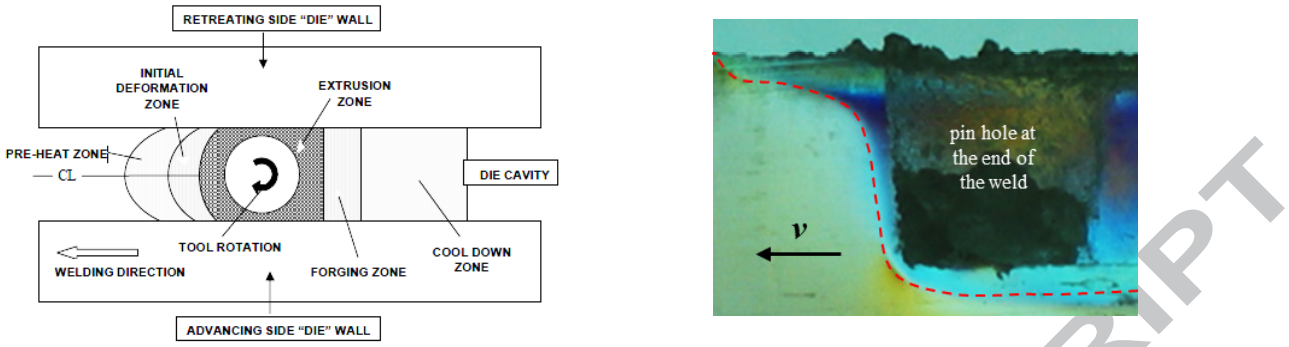

Figure 9 - Schematic representation of Arbegast model [14] for FSW of metals (a) and longitudinal sections of tool 1 sample (b)

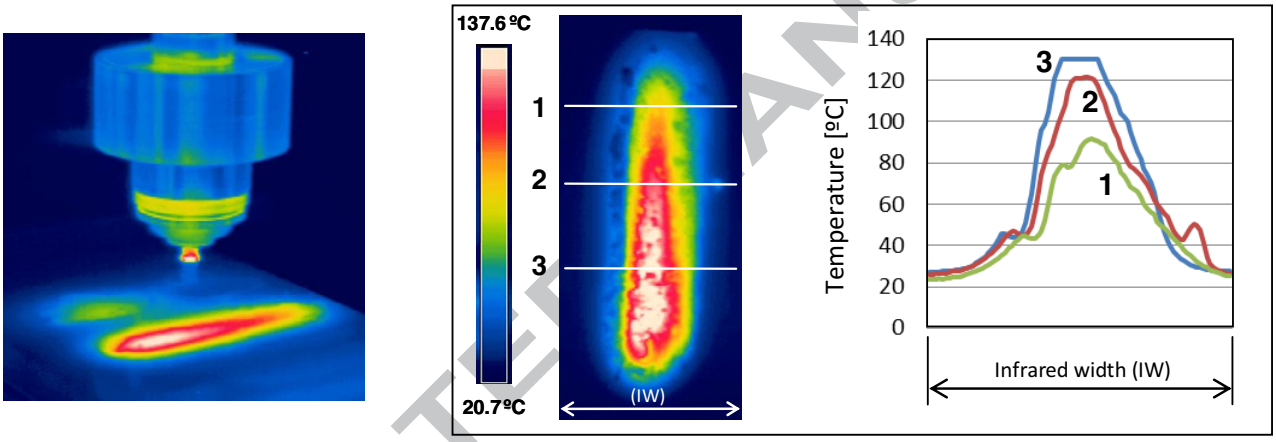

Figure 10 - Tool and material image captured with a infrared camera after FWS (a) and temperature fields surface and temperature profile at different weld positions (b)

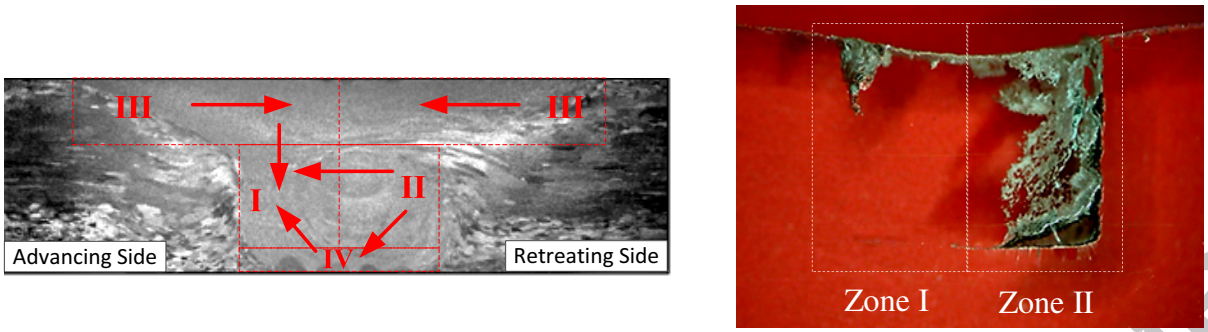

(a) (b)

Figure 11 - Representation of deformation zones and flow material for FSW of metals according Arbegast model (a) and transverse sections of Tool 1 sample (b)

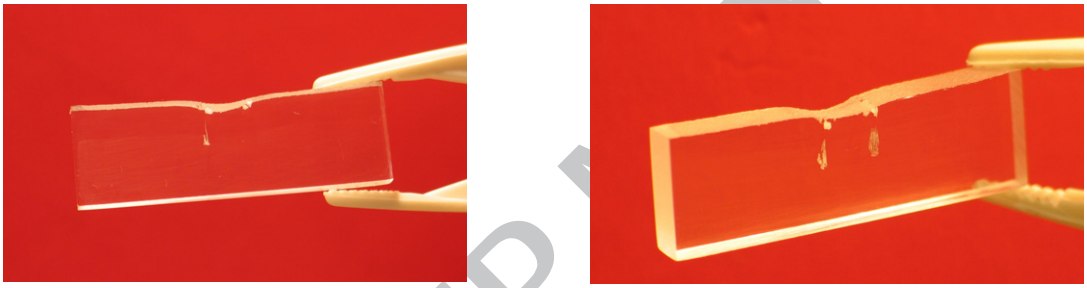

(a) (b)

Figure 12 - Optical microscopy image of the sample after welding (a) and image of the weld one month after welding (b) showing additional defects.

Highlights

- Analyses of polymers thermo-mechanical conditions during FSW;
- Application of Arbegast partitioned material flow model;
- Analysis of PMMA welds morphology and defects;
- Qualitative assessment of residual stress fields;
- Temperature distribution during FSW;